An Investigation of the Transmission System of a Tendon Driven Robot Hand

Ali Nahvi, John M. Hollerbach, Yangming Xu, and Ian W. Hunter

Biorobotics Laboratory, McGill University
3775 University St., Montreal, Quebec, Canada H3A 2B4

Abstract

The transmission system of the Utah/MIT Dextrous Hand (UMDH) is investigated theoretically and experimentally. It is shown that the friction of the routing pulleys is not negligible and should be considered in the force control of the UMDH. In the frequency range of the pneumatic actuators (80Hz), tendons act like springs and the first mode of the tendons is above that frequency range.

1 Introduction

Mechanical properties, such as nonlinear friction, damping, hysteresis, compliance, and nonlinear dynamic behavior may be the major limiting factors in the force control of mechanisms. This is particularly the case for dextrous robot hands which employ complex tendon transmission systems. Partly as a result, experimental results on grasping are not nearly as advanced as grasping theories. To implement a suitable force control strategy, it is essential to fully understand the mechanical characteristics of the transmission system.

Most dextrous hand designs feature tendon transmission systems. Tendons pass either on the pulleys or through sheaths. Pulleys are attractive because they have lower friction than guide tubes, but require mounting surfaces and are less reliable. Guide tubes do not require any mounting surfaces, but introduce more friction.

Townsend [13] studied the effect of Coulomb and stiction on force control with integral feedback. He found that Coulomb friction may lead to an input dependent stability. Kaneko et al. [7] also discussed the input-dependent stability observed during the torque control of a dextrous hand with tendon-sheath system. They found that the friction and compliance existing in the tendon-sheath systems, bring a hysteresis into the dependence of joint torques and actuator displacement. They stated that the transmission characteristics is close to the gear backlash. They confirmed that there are close relationships between the input-dependent backlash and stability.

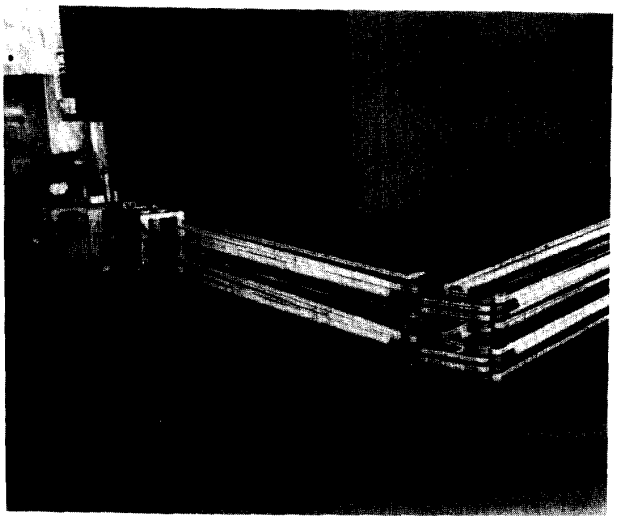

Figure 1: The Utah/MIT Dextrous Hand (UMDH).

In [8], the terms of apparent tendon-stiffness and equivalent backlash were defined for the tendon-sheath systems. They stated that the apparent tendon stiffness changes depend on whether the tendon is pulled or loosened. This eventually causes a direction-dependent response for force control. In [14], stiffness control is discussed for a robot finger with tendon-sheath transmission system. They considered dry friction and damping in the controller design. Rockenbeck [11] made some experiments to find the mass of an object held by the UMDH. He found that the effect of friction in the transmission is considerable. Johnstun and Smith [5] considered dynamics of tendons with an approach which uses the water hammer equations in the fluids. They also studied the pulley friction and found it to be primarily Coulombic.

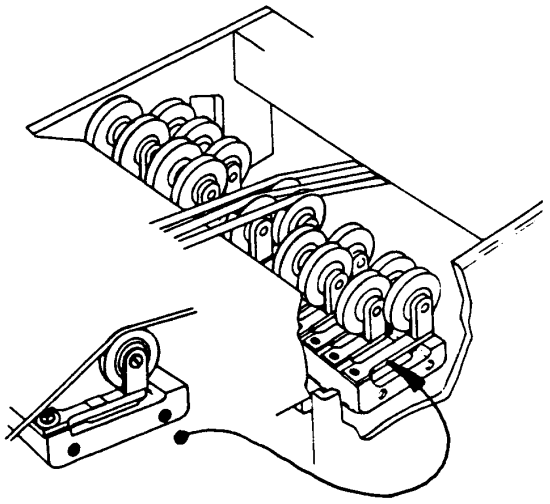

Figure 2: Tendon tension sensors located in the wrist of the UMDH [4].

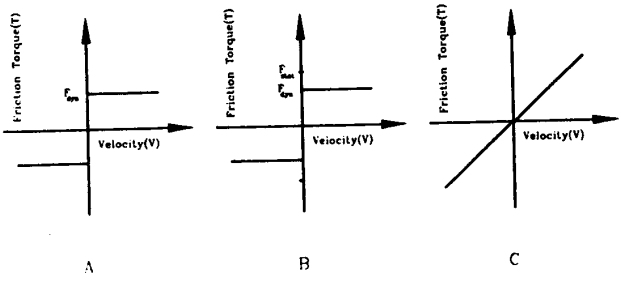

Figure 3: Common models of friction.

2 Modeling

2.1 System Description

The Utah/MIT Dextrous Hand (UMDH) [4] consists of four parts:

1) Hand: It has three 4-DOF fingers and an opposing 4-DOF thumb. Each finger has three parallel axis joints to provide curling motion and a proximal joint for abduction/adduction motion. Each finger joint is activated by a pair of opposite tendons. Joint angles are measured by Hall effect sensors with a linearity within 5 percent.

2) Wrist: It includes two perpendicular axes, implemented by a crossed yoke mechanism. The tendon tension measurement is also implemented in this area.

Figure 2 illustrates one of the 32 tendon tension sensing systems. The pulley is positioned in order to perturb the path of the tendon such that tendon tension imposes a load on the cantilevered beam. A semiconductor strain gauge bridge detects beam strain and provides a linear output for tendon tensions from 0 to 130 N. Supporting electronics are located in the Low Level Control System (LLCS).

3) Remotizer: The remotizing system includes 32 tendon pathways in four subsystems, each of which includes a series of longitudinal rods, rolling joints, and tendons. The longitudinal rods support the compressive stresses imposed by tendons and the system of rolling joints permit motion of the remotizer without altering tendon path lengths. The remotizer is a passive system which allows the UMDH to be freely positioned in space while receiving substantial energy from the actuator package. A third axis of rotation of the wrist is provided by axial rotation of the remotizer compression rods. Each rolling joint of remotizer includes 16 pulleys for tendon routing. The entire remotizer, wrist, and hand include 359 molded plastic pulleys with bearings. 347 of these pulleys have diameter of 12.4 mm, 8 have diameter of 18.3 mm, and 4 have diameter of 9.7 mm. The number of pulleys from the actuator to the tendon tension sensors is 248; all of them are 12.4 mm in diameter.

The tendon was made of a 12-strand braid of polyethylene fibers manufactured by Allied Fibers and marketed under the trade name of SPECTRA^R 1000. It is ultra-tough and high abrasion resistant. Some of the SPECTRA^R 1000 properties are as follows:

Density = 970 Kg/m^3,

Strength = 3.0 GPa.

4) Electropneumatic Actuators: Each tendon is driven by a single-stage, jet pipe valve attached to a glass cylinder housing a low-stiction graphite piston and steel rod. A rigorous description of these actuators can be found in [2].

2.2 Friction

Figure 3 shows three main models for friction [13]. The static and dynamic coefficients of friction are assumed to be the same in figure 3.A and different in figure 3.B (stiction). Figure 3.C shows linear viscous damping. A combination of these three types of friction is also possible. For example, we can express the combination of Coulomb and viscous friction which is applied on the tendon by a pulley as:

$$\begin{cases} T_f = -\mu F_n \frac{d}{2} sgn(v) - b\omega sgn(v) & if \quad v \neq 0 \\ \mid T_f \mid \leq \mu F_n \frac{d}{2} & if \quad v = 0 \end{cases} \quad (1)$$

where T_f is the frictional torque, μ is the coefficient of friction, F_n is the normal force applied on the pulley by the tendon, d is the bore diameter of the bearing, v is the tendon velocity, ω is the angular velocity, $sgn(v)$ is the sign of v, and b is the angular damping factor. A more rigorous modeling for friction which uses the static, dynamic, and damping friction can be found in [1]. The selection of the proper model for each system depends on its behavior and can be found by doing experiments as in this paper.

2.3 Tendon Dynamics

Johnstun and Smith [5],[6] developed a formulation for tendon dynamics similar to the hydraulic transmission line equations for a water hammer and also equations for electric transmission lines. We use their formulation with some modification.

Let's assume a tendon with length L and two forces and velocities at each end. Then in the Laplace domain:

$$F(0,s) = F_1(s) \tag{2}$$

$$V(0,s) = V_1(s) \tag{3}$$

$$F(L,s) = F_2(s) \tag{4}$$

$$V(L,s) = V_2(s) \tag{5}$$

where $F(0,s)$ is the tendon tension at the beginning of the tendon, and $F(L,s)$ is the tendon tension at the end. $V(0,s)$ and $V(L,s)$ represent the corresponding velocities at each end. Transmission line equations based on the model used in [10] can be obtained as:

$$\begin{bmatrix} V_1(s) \\ F_1(s) \end{bmatrix} = \begin{bmatrix} cosh\Gamma(s) & -sinh\Gamma(s)/Z \\ -Zsinh\Gamma(s) & cosh\Gamma(s) \end{bmatrix} \begin{bmatrix} V_2(s) \\ F_2(s) \end{bmatrix} \tag{6}$$

or:

$$\begin{bmatrix} V_2(s) \\ F_2(s) \end{bmatrix} = \begin{bmatrix} cosh\Gamma(s) & sinh\Gamma(s)/Z \\ Zsinh\Gamma(s) & cosh\Gamma(s) \end{bmatrix} \begin{bmatrix} V_1(s) \\ F_1(s) \end{bmatrix} \tag{7}$$

where:

$$\begin{aligned} \Gamma(s) &= Ls\sqrt{\frac{\rho}{k}} \\ Z &= \sqrt{\rho k} \end{aligned} \tag{8}$$

ρ is the mass of tendon per length, k is the normalized stiffness and defined as the product of the stiffness and the length of the tendon. Note that the tendon is assumed to be lossless in this model. k should be obtained experimentally and is a function of the tendon tension. Equations (6) and (7) are different from the corresponding equations of the water hammer and also those in [5],[6] because of a minus sign difference in the basic differential equations.

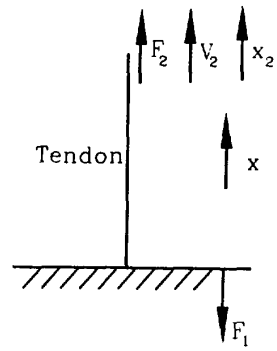

Figure 4: Tendon with a fixed end.

We use a special case where one end of the tendon is fixed (Figure 4). Because $V_1(s)$ is equal to zero and $sX(s) = V(s)$, then from (7):

$$sX_2(s) = \frac{1}{Z}sinh\Gamma(s)F_1(s) \tag{9}$$

$$\frac{F_1(s)}{X_2(s)} = \frac{sZ}{sinh\Gamma(s)} \tag{10}$$

$$F_2(s) = cosh\Gamma(s)F_1(s) \tag{11}$$

$$\frac{F_1(s)}{F_2(s)} = sech\Gamma(s) \tag{12}$$

In the UMDH, when the hand is in contact with an object, we can assume that each tendon is fixed at one end near the fingertip and the other end is pulled freely by an actuator. Then, (12) can be used to predict the dynamics of the force translation from the actuator side to the end-effector side.

3 Experimental Results

3.1 Coulomb's Friction of the Pulleys

We found that the use of some known masses is the best way to measure the coefficient of friction. We passed a tendon over several pulleys of the UMDH with equal diameters of 12.4 mm and attached some masses at the two ends of the tendon. We also found that the dynamic and the static coefficients of friction are so close to each other that they cannot be identified as two separate values. So, the assumption of stiction is obviated. The difference of weights at the two ends of the tendon and at the onset of movement was used in some static equations and μ found as:

$$\mu = 0.13 \tag{13}$$

In the above calculation, the bore diameter of 3 mm was considered for the pulleys.

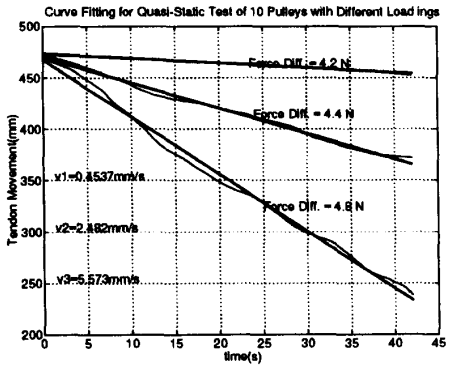

Figure 5: Movement of the tendon measured by the Optotrak.

3.2 Damping Coefficient of the Pulleys

We noticed that the velocity of the movement of the tendon in the above-mentioned setup was related to the weights. As we added masses at one end, we had a bigger velocity. Of course, this addition of masses also changed the value of the Coulomb friction because of more normal force on the pulleys. We used the Optotrak 3020 (Northern Digital, Ltd., Waterloo, Ontarion, Canada) to measure the velocity of the tendon. It has a stated accuracy of 0.1-0.15 mm in a 2.5 m distance and a resolution of 0.01 mm. One IRED (infrared emitting diode) was attached to the one end of the tendon and the sampling was done for different loadings for a duration of about 40 seconds (Figure 5). Notice that the velocity is almost constant for the three measurements done. Again from some equations relating Coulomb and damping friction, and also weights, we found b in (1) for the pulleys with diameter of 12.4 mm as:

$$b = 6.8 \times 10^{-4} N.m.s/rad \qquad (14)$$

Notice that we assume b to be independent of force and velocity.

3.3 Static Friction of the UMDH Transmission System

As we described earlier, the tendon tension is measured at the wrist of the UMDH. The friction is to be evaluated so that it can be fed forward for actuator control. An Entran Load Cell ELF-TC500-20 was attached to the tendon in the vicinity of the actuators to measure the tendon tension at the actuator side. Figure 6 shows the wrist force sensor measurement versus the tension near the actuators in a pull and release test. We increased cocontraction little by little and then decreased it. The figure shows a nonlin-

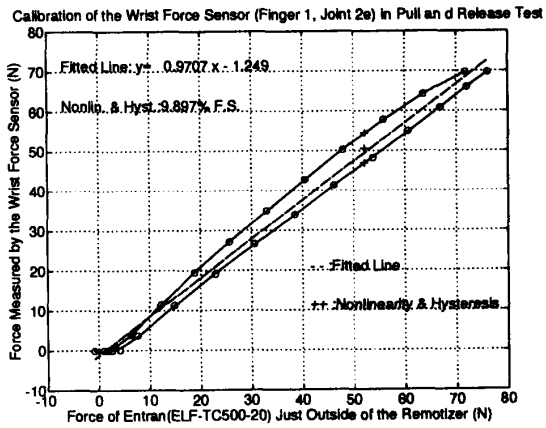

Figure 6: Hysteresis loop due to the remotizer pulleys.

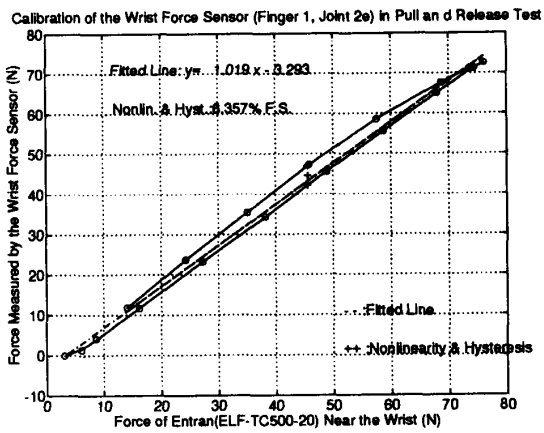

Figure 7: Hysteresis loop due to the two pulleys of the wrist.

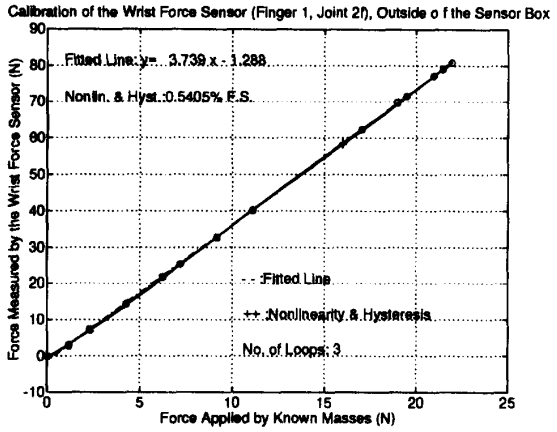

Figure 8: Hysteresis and nonlinearity of the wrist force sensor obtained from three loops.

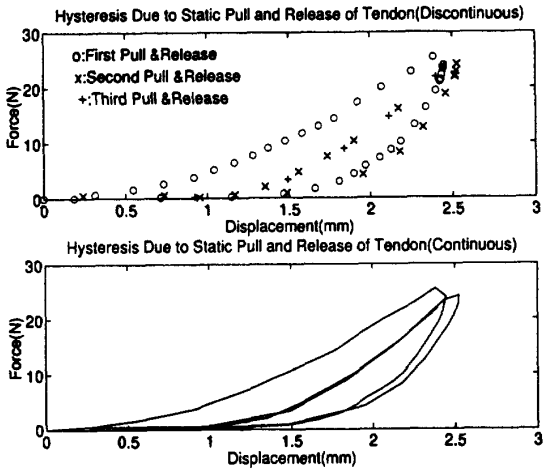

Figure 9: Displacement-domain hysteresis of the tendon.

earity and hysteresis of 9.9 percent of full scale due to the friction which is not negligible. A similar experiment was done by pulling the Entran load cell near the wrist (figure 7). As we expect, the value of the non-linearity and hysteresis becomes smaller (6.4 percent of F.S.). Notice that at the maximum point of tension (about 70 N), the actuator was saturated, and the friction was not in a specified direction, because the tendon had a little back and forth movement. Theoretically, it should have been flat at the extreme points.

3.4 Accuracy of the Wrist Force Sensor

We tested the accuracy of the wrist force sensors. Sensors were separated from the sensor box and tested by some known masses. Figure 8 shows very low nonlinearity and hysteresis of 0.54 percent of full scale which is quite promising. So, the error due to the wrist force sensor is negligible compared with the friction.

3.5 Stiffness and Displacement-Domain Hysteresis

As the tension is increased, the tendon fibers tend to align themselves in parallel. Intuitively, it can be imagined that the more tension, the stiffer the tendon. Figure 9 shows the result of several loops of pull and release of the tendon. It is seen from the figure that: a) Stiffness is increased with force and b) After a few times of pull and release, the displacement-domain hysteresis is obviated. Remember that this stiffness is a parameter of tendon dynamic equations.

3.6 Tendon Dynamics

To study the tendon dynamics, we used a setup as in figure 10. Tendon was excited at one end and fixed at the other end. The shaker is a linear electromagnetic actuator (Brüel and Kjær, model 4808) and applies perturbation with a bandwidth of 10 kHz. This actuator is driven by either single or dual power amplifiers. Movement of the actuator is measured by an inductive displacement transducer (Data Instruments, Fastar FS380) which has a flat frequency response up to 15 kHz [9]. The Entran force sensor was used to measure the force at the fixed end. It has a useful frequency up to 10 kHz. We did several tests using different lengths of tendon. All of the tests show that the first resonance frequency of a tendon as long as the UMDH tendons is beyond the obtainable bandwidth of the pneumatic actuators of the UMDH which is 80 Hz [3]. Figure 11 shows the bode plot of $\frac{F_1(s)}{X_2(s)}$ where F_1 is the force measured by the Entran load cell and X_2 is measured by the displacement transducer. At low frequencies, tendons act like a simple spring. This test was done for a 38cm tendon. The corresponding coherence function is shown in Figure 12 which is above 80% upto 600 Hz. We do not see any resonance up to this frequency in Figure 11. From (10), we notice that at the first resonance:

$$sinh\Gamma(j\omega) = 0 \Rightarrow jsin\Gamma(\omega) = 0 \qquad (15)$$

$$\Rightarrow \pi = L\omega\sqrt{\frac{\rho}{k}} \Rightarrow \omega = \frac{\pi}{L}\sqrt{\frac{k}{\rho}} \qquad (16)$$

So, the first resonance has an inverse relation with the length. Assuming a length of 1.5m for each tendon of the

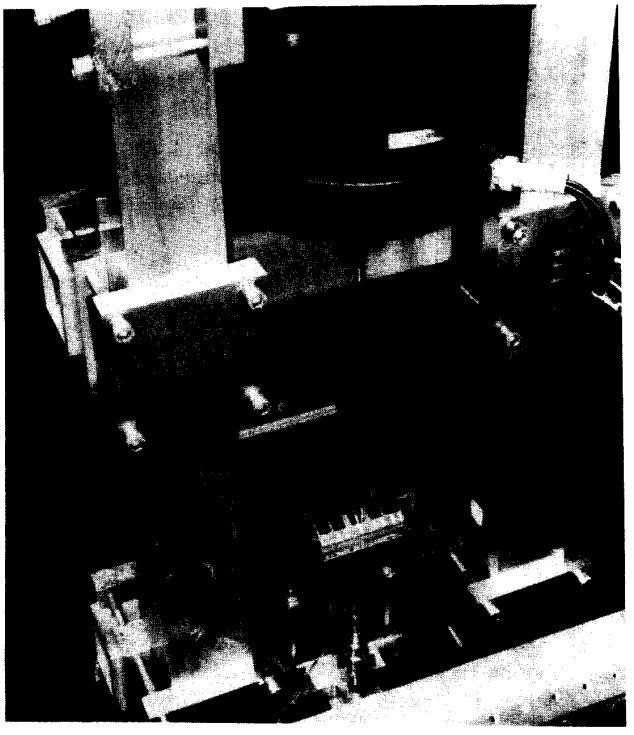

Figure 10: Dynamic testing setup.

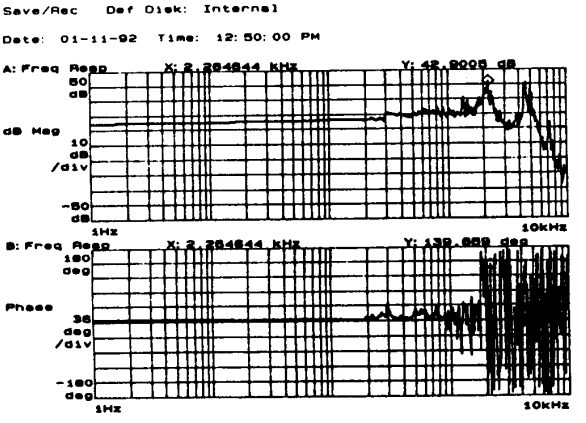

Figure 11: Bode plot of force to displacement (N.T.S.).

UMDH, the first resonance would be much higher than 150 Hz.

4 Conclusion

A comprehensive modeling and experimental identification of the transmission system of the UMDH was done to be used in the control system of the UMDH. It was shown that the friction of the pulleys used for routings of tendons is a combination of Coulomb and damping friction which are considerable relative to the tendon tensions. The effect of Coulomb friction was found to be higher than damping friction. The cocontraction of tendons has an essential effect on the Coulomb friction. Although researchers usually state that the friction of dextrous hands is considerable just in the tendon-sheath systems, but this paper shows that in the case of tendon-pulleys, the effect of friction should also be taken into account for the purpose of control.

As stated in [5], routing the tendon over several pulleys increases the overall damping in the system, but the effect is not too serious if pulleys have low-friction bearings. We would have much lower friction in the UMDH, if better bearings were used. However, even with the present bearings, the effect of friction is about one-fourth of that of tendon-sheath systems.

Because of the low frequency range of the UMDH, dynamic effects of the tendon can be neglected. The tendons act like springs at the working frequency range of the UMDH.

There are some factors which may change our model:

- The pulleys staggered together are not fixed axially. So, the amount of friction changes with the axial movement of pulleys.
- In some orientations of the remotizer, there is contact between the tendons and the longitudinal rods of the remotizer.
- In some pulleys, tendons approach the pulleys not quite perpendicularly to the axes of the pulleys. This also can be a source of friction.

Acknowledgments

Support for this research was provided by the Natural Sciences and Engineering Research Council (NSERC) Network Centers of Excellence Institute for Robotics and Intelligent Systems (IRIS). Personal support for JMH was provided by the NSERC/Canadian Institute for Advanced Research (CIAR) Industrial Chair in Robotics. The first author was funded by the Ministry of Culture and Higher Education of Iran.

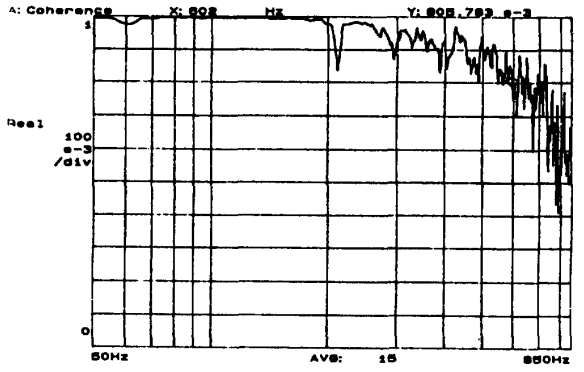

Figure 12: Coherence of force and displacement signals.

References

[1] Armstrong-Hélouvry, B., "Stick slip and control in low-speed motion," *IEEE Transactions on Automatic Control*, vol. 38, no. 10, pp. 1483-1496, 1993.

[2] Henri, P.D., Study of a Jet Pipe Electropneumatic Actuator, M.Eng. Thesis, McGill Univ., Dept. of Biomedical Eng., 1994.

[3] Henri, P.D., and Hollerbach, J.M., "An analytical and experimental investigation of a jet pipe controlled electropneumatic actuator," in *Proc. IEEE Int. Conf. Robotics and Automation*, pp. 300-307, 1994.

[4] Jacobsen, S.C., Iversen, E.K., Knutti, D.F., Johnson, R.T., and Biggers, K.B., "Design of the Utah/MIT Dextrous Hand," in *Proc. IEEE Int. Conf. Robotics and Automation*, San Francisco, pp. 1520-1532, April 7-10, 1986.

[5] Johnstun, C.R., and Smith, C.C., "Modeling and design of a mechanical tendon actuation system," *Trans. ASME J. Dynamic Systems, Measurement and Control*, vol. 114, pp. 253-261, 1992.

[6] Johnstun, C.R., Model and Design of a Mechanical Tendon System, M.Sc. Thesis, Brigham Young University, Dept. of Mechanical Engineering, February, 1989.

[7] Kaneko, M., Paetsch, W., and Tolle, H., "Input-dependent stability of joint torque control of tendon-driven robot hands," *IEEE Trans. Industrial Electronics*, vol. 39, pp. 96-104, 1992.

[8] Kaneko, M., Wada, M., Maekawa, H., and Tanie, K., "A new consideration on tendon-tension control system of robot hands," in *Proc. IEEE Intl. Conf. Robotics and Automation*, Sacramento, pp. 1028-1033, April 9-11, 1991.

[9] Lafontaine, S., Cai, K., and Hunter, I.W., "Temperature dependence of NiTi fiber impedance," in *18th Canadian Medical and Biological Engineering Conference*, 1985.

[10] Paynter, H.M., "Fluid transients in engineering systems," *Handbook of Fluid Dynamics*, edited by Streeter, V.L.. NY: McGraw-Hill, pp. 20-1 - 20-47, 1961.

[11] Rockenbeck, W.H., Static Load Estimation Using the Utah/MIT Dextrous Hand, B.Sc. Thesis, M.I.T., Dept. of Electrical Engineering and Computer Science, May, 1989.

[12] Salisbury, J.K., and Craig, J.J., "Articulated hands: force control and kinematic issues," *Int. J. Robotics Research*, vol. 1, no. 1, pp. 4-17, 1982.

[13] Townsend, W.T., "The Effect of Transmission Design on Force-Controlled Manipulator Performance," Technical Report 1054, MIT Artificial Intelligence Lab, 1988.

[14] Vossoughi, R., and Donath, M., "Robot finger stiffness control in the presence of mechanical nonlinearities," *Trans. ASME J. Dynamic Systems, Meas. & Control*, vol. 110, pp. 236-245, 1988.